

Port-LLM: A Port Prediction Method for Fluid Antenna based on Large Language Models

Yali Zhang, Haifan Yin, *Senior Member, IEEE*, Weidong Li, Emil Björnson, *Fellow, IEEE* and Mérouane Debbah, *Fellow, IEEE*

Abstract—The objective of this study is to address the mobility challenges faced by User Equipment (UE) through the implementation of fluid antenna (FA) on the UE side. This approach aims to maintain the time-varying channel in a relatively stable state by strategically relocating the FA to an appropriate port. To the best of our knowledge, this paper introduces, for the first time, the application of large language models (LLMs) in the prediction of FA ports, presenting a novel model termed Port-LLM. The proposed method consists of two primary steps for predicting the moving port of the FA: the first involves utilizing the channel tables that encompass historical channel state information from all movable ports of the FA to forecast the channel tables for subsequent time periods; the second step entails selecting the port of the FA for the forthcoming time based on the predicted channel tables and the known reference channels that require alignment. To enhance the learning capabilities of the LLM model in the context of FA port prediction, we incorporate the Low-Rank Adaptation (LoRA) fine-tuning technology. Furthermore, during the model training phase, we implement the warm-up-aided cosine learning rate (LR) technique to augment the accuracy of the predictions. The simulation results show that our model exhibits strong generalization ability and robustness under different numbers of base station antennas and medium-to-high mobility speeds of UE. In comparison to existing FA port calculation methods, the performance of the port predicted by our model demonstrates superior efficacy. Additionally, our model exhibits lower prediction costs and faster prediction and reasoning speeds.

Index Terms—Fluid antennas, large language models, channel prediction, moving port prediction, Port-LLM.

I. INTRODUCTION

In recent decades, the implementation of Multiple-Input Multiple-Output (MIMO) technology has significantly enhanced the capacity and reliability of communication systems. Nevertheless, the fixed deployment of current antennas limits the utilization of spatial degrees of freedom (DoF), particularly in environments with little scattering. Additionally, the constraints imposed by the antenna spacing, i.e.,

the half-wavelength limitation, further restrict the number of antennas that can be deployed within a confined space. This limitation is particularly pronounced on the UE side, where the spatial dimensions are typically small, resulting in inadequate exploitation of narrow space diversity [1]–[3]. In contrast, a novel antenna technology known as the fluid antenna (FA) or movable antenna, depending on the hardware implementation, offers the capability to switch among various positions, referred to as “ports”, within a specified area. In this paper, the terms “Fluid antenna” and “Movable antenna” are considered interchangeable. In the subsequent discussion, we will employ the term “Fluid antenna” to encompass both concepts. The position and configuration of the FA can be dynamically adjusted, allowing for greater adaptability [4], [5]. Despite the limited size of the movable area of the FA, the potential for numerous movable ports allows for significant diversity gain across a multitude of spatially dependent ports. Furthermore, the continuous mobility of the FA within a specified area facilitates the optimal exploitation of spatial DoF, thereby enhancing the conditions of the wireless channel.

The fluid antenna system (FAS) presents significant advantages and potential applications [6]. Notably, the integration of FAS with MIMO technology, referred to as MIMO-FAS, has the capacity to enhance the performance of a MIMO system by selecting ports that enhance the beamforming gain or improve the MIMO rank conditions, thereby facilitating exceptionally high data transmission rates and enhanced reliability. In multi-user scenarios, FAS can be employed for interference suppression purposes, allowing users to leverage naturally occurring interference nulls in the propagation environment by adjusting the FA port, which reduces the need for interference-suppression precoding at the BS. Furthermore, FAS can be integrated with Reconfigurable Intelligent Surface (RIS) technology, thereby circumventing the need for intricate optimization processes associated with RIS [7], [8].

FAS also encounters numerous challenges [6], one of which pertains to the selection of ports. The advantages of FAS compared to conventional fixed-location antenna systems (FPAs) are primarily due to its flexible antenna positioning capabilities. Nevertheless, identifying the appropriate port for the FA to achieve superior communication performance presents a significant challenge, as the channel response exhibits a significant degree of nonlinearity as a function of the spatial positioning of the FA. Conventional optimization techniques for FAS port selection encompass the gradient descent [9] method, successive convex approximation (SCA) [10], alternating optimization (AO) method, exhaustive search method,

Yali Zhang, Haifan Yin and Weidong Li are with School of Electronic Information and Communications, Huazhong University of Science and Technology, 430074 Wuhan, China (email: yalizhang@hust.edu.cn; yin@hust.edu.cn; weidongli@hust.edu.cn).

E. Björnson is with the Division of Communication Systems, KTH Royal Institute of Technology, Stockholm, Sweden. E-mail: emilbjo@kth.se.

M. Debbah is with KU 6G Research Center, Department of Computer and Information Engineering, Khalifa University, Abu Dhabi 127788, UAE (email: merouane.debbah@ku.ac.ae) and also with CentraleSupélec, University Paris-Saclay, 91192 Gif-sur-Yvette, France.

The corresponding author is Haifan Yin.

This work was supported by the Fundamental Research Funds for the Central Universities and the National Natural Science Foundation of China under Grant 62071191. E. Björnson was supported by the Grant 2022-04222 from the Swedish Research Council.

etc. Nevertheless, these approaches either necessitate precisely known channel state information (CSI) or entail significant time and computational resources to identify an appropriate port.

The issue of mobility, referred to as the curse of mobility [11], has consistently been a significant concern within the field of communications. The movement of the UE can introduce a significant Doppler effect, leading to the obsolescence of the communication channel. If the BS performs precoding design with the outdated CSI, it may result in a decline in system performance. To address this mobility challenge, the work in [11] proposed the Vec Prony method and PAD method for channel prediction. Their findings indicate that it can achieve performance levels comparable to stationary scenarios with unaltered channels. As research in FAs has progressed, the paper [12] proposed utilizing the FA to mitigate mobility issues. Their study introduces an algorithm called ‘‘MPMP’’, which facilitates the port selection for FA. Empirical results demonstrate that the MPMP method outperforms the Vec Prony algorithm in both medium and high mobility scenarios.

Deep learning (DL) technology has garnered significant interest within the domain of wireless communication, owing to its robust capabilities in feature extraction and modeling [13]. This has led to notable advancements, including the application of DL for tasks such as channel prediction, solving beamforming vector [14], antenna selection (AS) [15], etc. From these applications, it is evident that applying DL technology to FA port prediction to address mobility issues has great potential, since wireless channels have much structure even if it is hard to model. According to the research conducted by the paper [12], the port selection for FA is inherently a time-sensitive issue. Techniques such as Recurrent Neural Networks (RNNs) [16], Long Short-Term Memory (LSTM) [17] network, and Gated Recurrent Unit (GRU) [18] are frequently employed to tackle problems characterized by temporal variations. However, these traditional neural network models designed for time series analysis typically exhibit a small architecture and possess a limited number of internal learnable parameters. Consequently, their capacity to model complex problems is constrained. Furthermore, these models demonstrate limited generalization capabilities and exhibit heightened sensitivity to variations in environmental parameters, thereby constraining their practical applicability in real-world scenarios.

Large Language Models (LLMs), such as GPT-1, GPT-2 [19], GPT-3, and LLaMa, have significantly transformed the fields of natural language processing (NLP) and artificial intelligence (AI). Currently, researchers have initiated investigations into the application of LLMs within the physical layer of wireless communication networks. Notable examples include the Csi-LLM [20] and LLM4CP [21] models, which have been developed for channel prediction, as well as proposals for utilizing LLMs in beam prediction tasks [22]. However, there is a notable gap in the literature regarding the application of LLMs for port prediction in FA. This paper addresses this gap by proposing an FA port prediction model that leverages LLMs. However, given that the extensive datasets utilized for the pre-training of LLMs predominantly consist of diverse

textual data, these models lack the capability to interpret wireless communication data. As a result, aligning wireless communication data with natural language data remains a significant challenge when implementing LLMs within the physical layer of wireless communication networks.

In this article, we introduce an FA port prediction model, designated as Port-LLM, to tackle the challenges associated with mobility. Our objective is to maintain a relatively stable channel despite the movement of the UE by relocating the FA to the port predicted by our model at each moment. The foundational architecture of our model is derived from the pre-trained GPT-2 [19] framework, and we employ LoRA [23] technology to fine-tune the loaded GPT-2 model. The research presented in [12] indicates that the critical factor in selecting ports for FA lies in the precise forecasting of CSI pertaining to all movable ports of the FA on the UE side at any given moment. As a result, our proposed LLM-based FA port prediction model utilizes the CSI corresponding to all movable ports on the UE side from the preceding T moments, referred to as the ‘‘channel tables,’’ as input. Subsequently, the proposed Port-LLM is employed to forecast the channel tables for the subsequent F moments. Ultimately, the moving ports of the FA at the subsequent F moments are derived from the channel tables predicted by our model, in conjunction with the known reference channels that require alignment. Generally, the process of utilizing the proposed Port-LLM for FA port prediction can be categorized into two primary phases: the first phase involves channel prediction, while the second phase pertains to port selection.

The main contributions of this paper are as follows:

- This paper represents the first application of LLMs to the task of FA port selection, introducing an innovative LLM-based FA port prediction model, referred to as Port-LLM. Our model utilizes the channel tables associated with all movable ports of the FA over a preceding period of T time intervals as input, and subsequently predicts the moving ports of the FA for the forthcoming F time intervals. By repositioning the FA to the port predicted by our model at each time, we aim to keep the time-varying channel approximately constant.
- To ensure that the wireless communication data pertinent to this task is aligned with the data patterns of the pre-trained LLM, we developed a specialized module for data processing. Concurrently, we conducted LoRA fine-tuning on the GPT-2 model. By employing low-rank matrix techniques, the LoRA fine-tuning approach significantly diminishes the number of parameters required for retraining our model on this specific task, while preserving the knowledge acquired during the pre-training phase of the GPT-2 model.
- We introduce the warm-up-aided cosine LR scheduler within the training process of the proposed model, which greatly improves the prediction accuracy and convergence speed of our model.

Notation: We use boldface to denote matrices and vectors. \mathbb{R}^n and \mathbb{C}^n denote the spaces of n -dimension real and complex numbers, respectively. $(\cdot)^T$ represents the transpose. $\text{argmin}(\cdot)$

refers to the input parameter that minimizes the objective function. $\text{unravel_index}(p, (n, m))$ denotes the multi-dimensional coordinates associated with the integer p within an $n \times m$ dimensional matrix. $|\cdot|$ is the absolute value, $\|\cdot\|$ represents the Euclidean norm, and $\mathbb{E}[\cdot]$ represents the expectation operator.

II. SYSTEM MODEL

We consider a time division duplexing (TDD) system, where a BS with an $N_y \times N_z$ uniform planar array (UPA) serves a certain UE that is equipped with an FA. The setup is illustrated in Fig. 1.

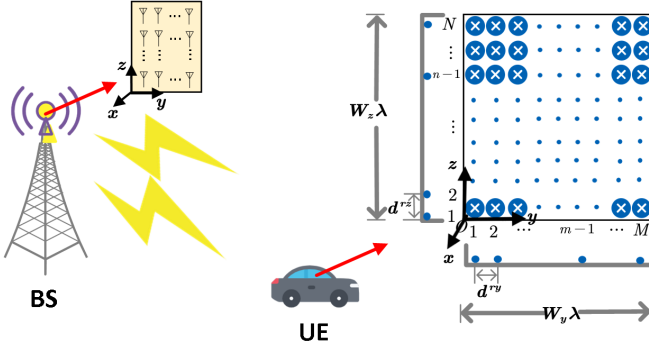


Fig. 1: The FA-assisted DL wireless communication system.

The placement of the antennas on the BS side is static, with the antenna panel situated within the yOz plane. The spacing between the antennas on the panel, along the y -axis and z -axis, is denoted by d^{ry} and d^{rz} , respectively. Conversely, the UE-side antenna is capable of movement within the yOz plane, characterized by a moving area of $W_y \lambda \times W_z \lambda$, where $W_y \lambda$ and $W_z \lambda$ denote the permissible displacements along the y -axis and z -axis, respectively. The symbol $\lambda = \frac{c}{f_c}$ denotes the wavelength, while c and f_c represent the speed of light and the carrier frequency, respectively. It is assumed that, on the UE side, the quantities of movable antenna ports along the y -axis and z -axis are denoted by M and N , respectively. The inter-port distances are defined as follows:

$$d^{ry} = \frac{W_y \lambda}{M-1} = \frac{\lambda}{\rho_y}, \quad (1)$$

$$d^{rz} = \frac{W_z \lambda}{N-1} = \frac{\lambda}{\rho_z}, \quad (2)$$

where $\rho_y = \frac{M-1}{W_y}$ and $\rho_z = \frac{N-1}{W_z}$ are utilized to represent the port density along the y -axis and z -axis, respectively.

On the BS side, the coordinate position vector of the k -th antenna is

$$\mathbf{d}_k^{\text{tx}} = [0, d^{ry}(n_y - 1), d^{rz}(n_z - 1)]^T, \quad (3)$$

where $1 \leq n_y \leq N_y, 1 \leq n_z \leq N_z$. And $1 \leq k \leq N_t, N_t = N_y \times N_z$.

On the UE side, the coordinate position vector of the antenna located at the (n, m) -th port is represented as

$$\mathbf{d}_{n,m}^{\text{rx}} = [0, d^{ry}(m-1), d^{rz}(n-1)]^T, \quad (4)$$

where $1 \leq m \leq M, 1 \leq n \leq N$. The spherical unit vectors on the BS and UE sides are:

$$\mathbf{r}^{\text{tx}} = \begin{bmatrix} \sin \theta_{\text{EOD}} \cos \phi_{\text{AOD}} \\ \sin \theta_{\text{EOD}} \sin \phi_{\text{AOD}} \\ \cos \theta_{\text{EOD}} \end{bmatrix}, \quad (5)$$

$$\mathbf{r}^{\text{rx}} = \begin{bmatrix} \sin \theta_{\text{EOA}} \cos \phi_{\text{AOA}} \\ \sin \theta_{\text{EOA}} \sin \phi_{\text{AOA}} \\ \cos \theta_{\text{EOA}} \end{bmatrix}, \quad (6)$$

where $\theta_{\text{EOA}}, \phi_{\text{EOA}}, \theta_{\text{EOD}}, \phi_{\text{EOD}}$ correspond to the elevation angle of arrival (EOA), azimuth angle of arrival (AOA), elevation angle of departure (EOD), and azimuth angle of departure (AOD), respectively. Furthermore, $\theta_{\text{EOA}}, \theta_{\text{EOD}} \in [0, \pi]$ and $\phi_{\text{AOA}}, \phi_{\text{AOD}} \in (-\pi, \pi]$. The Doppler frequency shift is denoted by $w = \frac{(\mathbf{r}^{\text{rx}})^T \mathbf{v}}{\lambda}$, where \mathbf{v} is a vector that represents the velocity of the UE.

Similar to the model used in the study [24], we consider a scenario that encompasses one line-of-sight (LoS) path and P non-line-of-sight (NLoS) paths. Therefore, the channel coefficient between the k -th antenna on the BS side and the UE side antenna at the (n, m) -th port at time t can be expressed as:

$$h_{(k,n,m)}(t) = \sum_{p=1}^{P+1} \alpha_p \beta_p e^{\frac{j2\pi(\mathbf{r}_p^{\text{rx}})^T \mathbf{d}_{n,m}^{\text{rx}}}{\lambda}} \times e^{\frac{j2\pi(\mathbf{r}_p^{\text{tx}})^T \mathbf{d}_k^{\text{tx}}}{\lambda}} e^{j2\pi w_p t} e^{j2\pi f \tau_p}, \quad (7)$$

where f is the frequency, while τ_p and w_p denote the delay and Doppler frequency shift of the p -th path, respectively. Moreover, β_p denotes the amplitude of the p -th path and

$$\alpha_p = \begin{cases} \sqrt{\frac{1}{K_R+1}}, & p \in \text{NLoS}, \\ \sqrt{\frac{K_R}{K_R+1}}, & p \in \text{LoS}, \end{cases} \quad (8)$$

where K_R is the Ricean K -factor.

Furthermore, at time t , the channel coefficient between all BS-side antennas and the UE-side antenna located at the (n, m) -th port can be represented as

$$\mathbf{h}_{(n,m)}(t) = [h_{(1,n,m)}(t), \dots, h_{(N_t,n,m)}(t)]^T = \mathbf{A} \mathbf{c}_{(n,m)}(t) \in \mathbb{C}^{N_t \times 1}, \quad (9)$$

where $\mathbf{A} = [\mathbf{a}(\theta_1^{\text{tx}}, \phi_1^{\text{tx}}), \mathbf{a}(\theta_2^{\text{tx}}, \phi_2^{\text{tx}}), \dots, \mathbf{a}(\theta_{P+1}^{\text{tx}}, \phi_{P+1}^{\text{tx}})] \in \mathbb{C}^{N_t \times (P+1)}$ represents the steering vectors of all paths. θ_p^{tx} and ϕ_p^{tx} denote the EOD and AOD of the p -th path, respectively. The 3-D steering vector of the p -th path is defined as

$$\mathbf{a}(\theta_p^{\text{tx}}, \phi_p^{\text{tx}}) = \mathbf{a}_y(\theta_p^{\text{tx}}, \phi_p^{\text{tx}}) \otimes \mathbf{a}_z(\theta_p^{\text{tx}}) \in \mathbb{C}^{N_t \times 1}, \quad (10)$$

where

$$\mathbf{a}_y(\theta_p^{\text{tx}}, \phi_p^{\text{tx}}) = [1, \dots, e^{j\frac{2\pi}{\lambda} \sin \theta_p^{\text{tx}} \sin \phi_p^{\text{tx}} d^{ry}(N_y-1)}]^T, \quad (11)$$

$$\mathbf{a}_z(\theta_p^{\text{tx}}) = [1, \dots, e^{j\frac{2\pi}{\lambda} \cos \theta_p^{\text{tx}} d^{rz}(N_z-1)}]^T. \quad (12)$$

Moreover, the vector $\mathbf{c}_{(n,m)}(t) \in \mathbb{C}^{(P+1) \times 1}$ is given by

$$\mathbf{c}_{(n,m)}(t) = [c_{(1,n,m)} e^{j2\pi w_1 t}, \dots, c_{(P+1,n,m)} e^{j2\pi w_{P+1} t}]^T, \quad (13)$$

where $c_{(p,n,m)} = c_p e^{j\frac{2\pi}{\lambda} [\sin \theta_p^x \sin \phi_p^x d^{rx} (m-1) + \cos \theta_p^x d^{rz} (n-1)]}$ and $c_p = \alpha_p \beta_p e^{j2\pi f \tau_p}$. θ_p^x and ϕ_p^x are the EOA and AOA of the p -th path, respectively.

At time t , when the UE antenna is positioned at the $(1, 1)$ -th port, the mathematical representation of the channel between all BS antennas and the UE antenna is

$$\mathbf{h}_{(1,1)}(t) = [h_{(1,1,1)}(t), \dots, h_{(N_t,1,1)}(t)]^T = \mathbf{A}\mathbf{c}_{(1,1)}(t). \quad (14)$$

Without loss of generality, we designate $\mathbf{h}_{(1,1)}(t)$ as the reference channel. At time $(t + \Delta t)$, the channel transitions to $\mathbf{h}_{(1,1)}(t + \Delta t)$ due to the mobility of the UE-side antenna.

At time $(t + \Delta t)$, we represent the channel coefficients associated with all ports as follows:

$$\mathbf{S}(t + \Delta t) = \{\mathbf{S}_1(t + \Delta t), \dots, \mathbf{S}_{N_t}(t + \Delta t)\} \in \mathbb{C}^{N_t \times N \times M}, \quad (15)$$

where

$$\mathbf{S}_i(t + \Delta t) = \begin{bmatrix} h_{(i,1,1)}(t) & \dots & h_{(i,1,M)}(t) \\ \vdots & \vdots & \vdots \\ h_{(i,N,1)}(t) & \dots & h_{(i,N,M)}(t) \end{bmatrix} \in \mathbb{C}^{N \times M}, \quad (16)$$

denotes the channel matrix between the i -th antenna at the BS and all ports of the FA at the time $(t + \Delta t)$.

The objective of our study is to identify a specific port, denoted by $(n_{\text{opt}}, m_{\text{opt}})$, at a future time $(t + \Delta t)$, from the entire set of available ports. This selection aims to ensure that when the UE side antenna slides to the $(n_{\text{opt}}, m_{\text{opt}})$ -th port, the channel information $\mathbf{h}_{(n_{\text{opt}}, m_{\text{opt}})}(t + \Delta t)$ closely aligns with the reference channel $\mathbf{h}_{(1,1)}(t)$, thereby keeping the channel approximate constant. We expand the $\mathbf{h}_{(1,1)}(t) \in \mathbb{C}^{N_t \times 1}$ in order to obtain the reference channel matrix corresponding to all ports as outlined below:

$$\mathbf{H}_{\text{ref}}(t) = \{\mathbf{H}_1(t), \dots, \mathbf{H}_{N_t}(t)\} \in \mathbb{C}^{N_t \times N \times M}, \quad (17)$$

where

$$\mathbf{H}_i(t) = \begin{bmatrix} h_{(i,1,1)}(t) & \dots & h_{(i,1,M)}(t) \\ \vdots & \dots & \vdots \\ h_{(i,N,1)}(t) & \dots & h_{(i,N,M)}(t) \end{bmatrix} \in \mathbb{C}^{N \times M}. \quad (18)$$

To maintain a relatively static channel, the following expression can be utilized to determine the moving port $(n_{\text{opt}}, m_{\text{opt}})$ of FA at time $(t + \Delta t)$:

$$(n_{\text{opt}}, m_{\text{opt}}) = \text{unravel_index} \left(\text{argmin} \left(\sum_{i=1}^{N_t} \left| \mathbf{S}_i(t + \Delta t) - \mathbf{H}_i(t) \right| \right), (N, M) \right). \quad (19)$$

The aforementioned formula indicates that when the reference channel is known, determining the moving port of FA at the subsequent moment for maintaining a relatively stable channel hinges on acquiring the channel matrices that connect all antennas on the BS side with all movable ports of the FA on the UE side at that particular moment. For the sake of clarity in the subsequent sections, we will call the channel matrix between the i -th antenna on the BS side and all movable ports of FA at a given time as a ‘‘channel table’’.

III. PORT-LLM

In this section, we propose a model for predicting the moving port of FA, referred to as Port-LLM, which is grounded in LLMs technology. The primary objective of our model is to ensure that the channel remains relatively stable by relocating the FA on the UE side to the anticipated port while the UE is in motion. To accomplish this, we initially employ the proposed Port-LLM model to forecast the channel tables $\hat{\mathbf{S}} = \{\hat{\mathbf{S}}_1, \dots, \hat{\mathbf{S}}_F\} \in \mathbb{C}^{F \times N \times M}$ for the subsequent F moments by utilizing the channel tables $\mathbf{S} = \{\mathbf{S}_1, \dots, \mathbf{S}_T\} \in \mathbb{C}^{T \times N \times M}$ from the preceding T moments. Subsequently, we proceed to utilize the predicted channel tables $\hat{\mathbf{S}} \in \mathbb{C}^{F \times N \times M}$ and the known reference channel $\mathbf{H}_{\text{ref}} \in \mathbb{C}^{F \times N \times M}$ to obtain the moving ports $\mathbf{P} = \{\mathbf{p}_1, \dots, \mathbf{p}_F\} \in \mathbb{R}^{F \times 2 \times 1}$ for the subsequent F moments.

A. Network Architecture

1) Data Preprocessing

To enhance the convergence rate during the training of our model, we initially apply mean-standard deviation normalization to the input data $\mathbf{S} \in \mathbb{C}^{T \times N \times M}$, i.e., $\tilde{\mathbf{S}} = \frac{\mathbf{S} - \mu}{\sigma}$, where μ and σ denote the mean and standard deviation of the input data, respectively. Given that neural network models typically operate on real-valued inputs and the input data \mathbf{S} is complex in nature, we decompose $\tilde{\mathbf{S}} \in \mathbb{C}^{T \times N \times M}$ into two components: the real part $\tilde{\mathbf{S}}_r \in \mathbb{R}^{T \times N \times M}$ and the imaginary part $\tilde{\mathbf{S}}_i \in \mathbb{R}^{T \times N \times M}$.

2) Input Embedding

To facilitate the extraction of features for subsequent modeling, we initially employ a linear layer to modify the dimensions of the tensor, thereby transforming $\tilde{\mathbf{S}}_r \in \mathbb{R}^{T \times N \times M}$ and $\tilde{\mathbf{S}}_i \in \mathbb{R}^{T \times N \times M}$ into $\tilde{\mathbf{S}}_r \in \mathbb{R}^{T \times d_{\text{model}}}$ and $\tilde{\mathbf{S}}_i \in \mathbb{R}^{T \times d_{\text{model}}}$, respectively. d_{model} is the feature dimension of the column vector in the matrix $\tilde{\mathbf{S}}_r$ or $\tilde{\mathbf{S}}_i$. Following this transformation, we implement the multi-head attention module [25] to extract features from both the real and imaginary components along the temporal dimension. For illustrative purposes, we will focus on the processing of the real component data $\tilde{\mathbf{S}}_r$ as an example. In this context, for each head $k \in \{1, \dots, K\}$ within the module, we define the query matrix, key matrix, and value matrix as $\mathbf{Q}_k^r = \tilde{\mathbf{S}}_r \mathbf{W}_k^Q$, $\mathbf{K}_k^r = \tilde{\mathbf{S}}_r \mathbf{W}_k^K$ and $\mathbf{V}_k^r = \tilde{\mathbf{S}}_r \mathbf{W}_k^V$, respectively. The reprogramming operation in each attention head is defined as

$$\mathbf{S}_k^r = \text{ATTENTION}(\mathbf{Q}_k^r, \mathbf{K}_k^r, \mathbf{V}_k^r). \quad (20)$$

Similarly, we also apply the K -head multi-head attention module to the imaginary part data $\tilde{\mathbf{S}}_i$:

$$\mathbf{S}_k^i = \text{ATTENTION}(\mathbf{Q}_k^i, \mathbf{K}_k^i, \mathbf{V}_k^i), \quad (21)$$

where \mathbf{S}_k^r and $\mathbf{S}_k^i \in \mathbb{R}^{T \times d}$. Subsequently, we will integrate the features derived from each head to obtain \mathbf{S}^r and $\mathbf{S}^i \in \mathbb{R}^{T \times d_{\text{model}}}$. In general, we set $d = d_{\text{model}}/K$. Ultimately, we will concatenate these two data to produce the data $\mathbf{X} \in \mathbb{R}^{T \times 2 \times d_{\text{model}}}$.

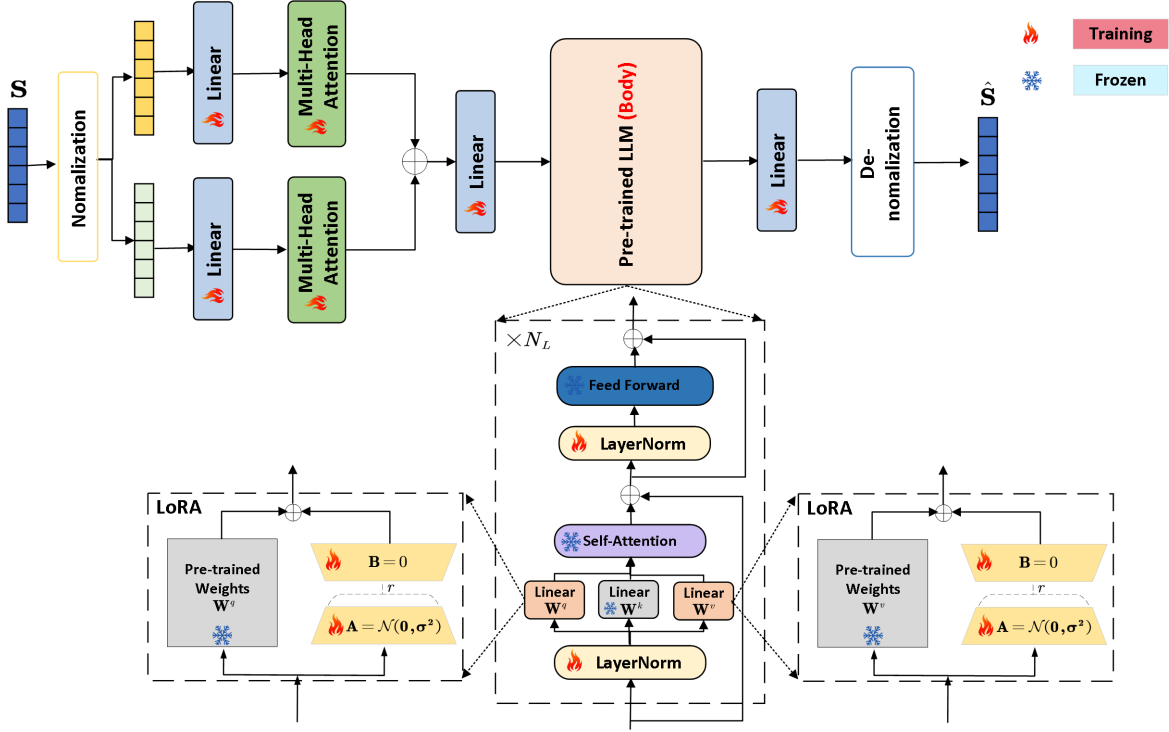


Fig. 2: The architecture of our proposed Port-LLM model.

3) Backbone network

Recent studies have demonstrated that fine-tuned LLMs can be effectively utilized within the physical layer of wireless communication systems, yielding impressive outcomes [20]–[22]. Motivated by these findings, we aim to leverage the robust modeling capabilities of the LLMs to accomplish our channel table prediction task, subsequently facilitating the port prediction for the FA.

The LLM selected for our study is the GPT-2 model [19]. We implement LoRA fine-tuning on the pre-trained GPT-2 model. LoRA fine-tuning is based on the intrinsic low-rank characteristics of the LLMs. It simulates full parameter fine-tuning by adding bypass matrices, aiming to achieve lightweight fine-tuning [23]. In particular, we exclusively conduct LoRA fine-tuning and retraining on the \mathbf{Q} and \mathbf{V} computations within the multi-head attention component of the GPT-2 model, while keeping the remaining model parameters frozen. This approach can substantially reduce the computational resources necessary for our model retraining and better utilize the knowledge acquired by GPT-2 during its pre-training phase. It is assumed that the input data for the module requiring LoRA fine-tuning is denoted by \mathbf{Z} . The process of LoRA fine-tuning is outlined as follows:

$$\mathbf{Q} = \mathbf{W}_Q \mathbf{Z} + \mathbf{B}_Q \mathbf{A}_Q \mathbf{Z} + \mathbf{b}_Q, \quad (22)$$

$$\mathbf{V} = \mathbf{W}_V \mathbf{Z} + \mathbf{B}_V \mathbf{A}_V \mathbf{Z} + \mathbf{b}_V, \quad (23)$$

where $\mathbf{W}_Q, \mathbf{W}_V \in \mathbb{R}^{d_m \times d}$ are the weights of the pre-trained GPT-2 model, which remain constant and are not subject to gradient updates throughout the training process. \mathbf{b}_Q and \mathbf{b}_V are the biases of the loaded model, which also remain

fixed. $\mathbf{B}_Q, \mathbf{B}_V \in \mathbb{R}^{d_m \times r}$ and $\mathbf{A}_Q, \mathbf{A}_V \in \mathbb{R}^{r \times d}$ are learnable parameters. Furthermore, $r \ll \min(d_m, d)$, resulting in negligible additional inference delay during model prediction when employing LoRA fine-tuning. As illustrated in Fig. 2, we employ random Gaussian initialization for parameter \mathbf{A}_Q and \mathbf{A}_V , and zero initialization for parameter \mathbf{B}_Q and \mathbf{B}_V prior to the commencement of our model training.

Generally, the data $\mathbf{X} \in \mathbb{R}^{T \times 2 \times d_{\text{model}}}$ is processed through a linear layer to modify its dimensionality to $\tilde{\mathbf{X}} \in \mathbb{R}^{F \times d_{\text{model}}}$ prior to being fed into the backbone network. Subsequently, the data is integrated into the backbone network, where the following procedure occurs:

$$\mathbf{X}_{\text{LLM}} = \text{LLM}_{\text{LoRA}}(\tilde{\mathbf{X}}) \in \mathbb{R}^{F \times d_{\text{model}}}, \quad (24)$$

where $\text{LLM}_{\text{LoRA}}(\cdot)$ represents the LLM-based backbone network that has been fine-tuned by LoRA.

4) Output Projection

In the output layer, a fully connected (FC) layer is employed in conjunction with a rearrange-tensor operation to derive the final output of the model by transforming the dimensions of \mathbf{X}_{LLM} in the following manner:

$$\mathbf{Y} = \text{rearrange}(\text{FC}(\mathbf{X}_{\text{LLM}})) \in \mathbb{R}^{F \times 2 \times N \times M}. \quad (25)$$

Subsequently, execute the denormalization process

$$\hat{\mathbf{Y}} = \sigma \mathbf{Y} + \mu, \quad (26)$$

where $\hat{\mathbf{Y}} \in \mathbb{R}^{F \times 2 \times N \times M}$. The second dimension corresponds to the real and imaginary components of the prediction channel tables, respectively. Additionally, the final output data $\hat{\mathbf{S}} \in \mathbb{C}^{F \times N \times M}$ is obtained as follows:

$$\hat{\mathbf{S}} = \hat{\mathbf{Y}}[:, 0, :, :] + j \hat{\mathbf{Y}}[:, 1, :, :]. \quad (27)$$

5) Moving Port prediction

Upon acquiring the channel tables $\hat{\mathbf{S}} = \{\hat{\mathbf{S}}_1, \hat{\mathbf{S}}_2, \dots, \hat{\mathbf{S}}_F\} \in \mathbb{C}^{F \times N \times M}$ for the subsequent F moments, we employ the predicted channel tables in conjunction with the associated known reference channel $\mathbf{H}_{\text{ref}} = \{\mathbf{H}_{\text{ref}_1}, \mathbf{H}_{\text{ref}_2}, \dots, \mathbf{H}_{\text{ref}_F}\} \in \mathbb{C}^{F \times N \times M}$ to derive the final predicted moving ports of the FA for the forthcoming F moments, utilizing the following formula:

$$\mathbf{p}_i = \text{unravel_index} \left(\underset{p}{\text{argmin}} \left(\left\| \hat{\mathbf{S}}_i - \mathbf{H}_{\text{ref}_i} \right\| \right), (N, M) \right), \quad (28)$$

where $\mathbf{P} = [\mathbf{p}_1, \dots, \mathbf{p}_F] \in \mathbb{R}^{F \times 2 \times 1}$, $\mathbf{p}_i = [n_i, m_i]^T \in \mathbb{R}^{2 \times 1}$, $1 \leq i \leq F$, $1 \leq n_i \leq N$, $1 \leq m_i \leq M$ denotes the predicted moving port of FA at the subsequent i -th moment. Here, n_i and m_i correspond to the port indices associated with the predicted moving port of FA along the z -axis and y -axis, respectively, at the subsequent i -th time instance.

B. Optimization objectives

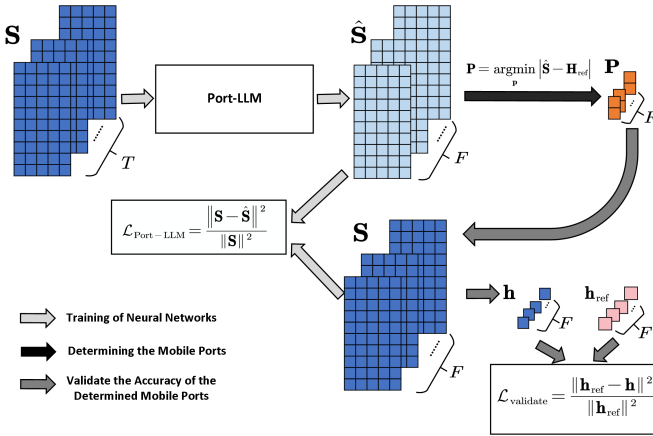


Fig. 3: The flowchart for predicting the moving ports of the FA based on our proposed model.

Our proposed model is initially trained on channel table datasets and then applied for testing. During the model training process, the objective function is the normalized mean square error (NMSE) between the channel tables $\hat{\mathbf{S}}$ predicted by our model for the future F moments and the actual channel tables \mathbf{S} for these F moments.

$$\mathcal{L}_{\text{Port-LLM}} = \frac{\|\mathbf{S} - \hat{\mathbf{S}}\|^2}{\|\mathbf{S}\|^2}. \quad (29)$$

The primary objective of this study is to forecast the moving ports of the FA for future time intervals. Attaining this objective necessitates the completion of two distinct phases. Firstly, we will employ our proposed neural network model to predict the channel tables for the forthcoming F time intervals, utilizing the channel tables from the preceding T time intervals as input. Subsequently, we will employ Eq. (28) to calculate the moving port of the FA corresponding to the specified future F time intervals. The comprehensive implementation procedure is illustrated in Fig. 3. The pseudocode for the algorithm predicting moving ports of the FA for future moments based on Port-LLM is outlined in **Algorithm 1**

Algorithm 1: A Port Prediction Method for Fluid Antenna based on the Proposed Port-LLM

Input: The channel tables at the last T moments \mathbf{S} , the corresponding reference channel tables \mathbf{H}_{ref}

Output: Predicted moving ports of FA at subsequent F moments \mathbf{P}

Initialization: Learning rate of our model $\alpha_{\text{Port-LLM}}$, exponential decay rate of moment estimates $\beta_{\text{Port-LLM}}$, batch size of the train sets m_1 , batch size of the test sets m_2 , the number of epochs \mathcal{K}

Process:

For epoch = 1, 2, \dots , \mathcal{K} **do**

- Forecast the channel tables for the future F time intervals $\hat{\mathbf{S}}$:

$$\hat{\mathbf{S}} = \text{Net}_{\text{Port-LLM}}(\mathbf{S})$$

- Update our proposed model by using adaptive moment estimation:

$$\mathcal{L}_{\text{Port-LLM}} = \frac{\|\mathbf{S} - \hat{\mathbf{S}}\|^2}{\|\mathbf{S}\|^2}$$

- Obtain the predicted moving ports of FA $\mathbf{P} = [\mathbf{p}_1, \dots, \mathbf{p}_F]$ for the subsequent F moments:

$$\mathbf{p}_i = \text{unravel_index} \left(\underset{p}{\text{argmin}} \left(\left\| \hat{\mathbf{S}}_i - \mathbf{H}_{\text{ref}_i} \right\| \right), (N, M) \right)$$

- Obtain the corresponding port channel $\mathbf{h} = [h_1, h_2, \dots, h_F]^T$ in the actual channel tables based on the predicted ports.

- Validate the accuracy of the predicted ports by our model, and calculate the NMSE between the channel of the port predicted by our model and the reference channel:

$$\mathcal{L}_{\text{validate}} = \frac{\|\mathbf{h}_{\text{ref}} - \mathbf{h}\|^2}{\|\mathbf{h}\|^2}$$

End for

IV. NUMERICAL RESULTS

This section will outline the simulation settings utilized for our model, assess its performance across various evaluation metrics, and conduct the comparative analysis with established methodologies for addressing FA moving ports.

A. Simulation Settings

1) Dataset

To mitigate the computational demands associated with the training of our model, we adopt a SISO system for the acquisition of training datasets. In this configuration, the antenna on the BS side remains stationary, while the UE side is equipped with the FA. This FA can move in a two-dimensional plane of dimensions $10\lambda \times 20\lambda$, situated within the y - z plane. The quantities of movable antenna ports along the y -axis and

TABLE I: The Main Simulation Parameters

Channel Model	CDL-D
Carrier Frequency (GHz)	39
CSI Delay (ms)	4
Delay Spread (ns)	616
Sampling Time	$T_0 = 5, 6, 10$
UE FA Configuration	$(W_y, W_z) = (10, 20)$, $(M, N) = (100, 50)$, $(\rho_y, \rho_z) = (5, 5)$
RMS Angular Spreads	$[31^\circ, 149^\circ, 150^\circ, 30^\circ]$, $[-38^\circ, 218^\circ, 227^\circ, -47^\circ]$, $[1^\circ, 179^\circ, 99^\circ, 81^\circ]$, $[10^\circ, 170^\circ, 36^\circ, 144^\circ]$, $[149^\circ, 31^\circ, 53^\circ, 127^\circ]$, $[129^\circ, 51^\circ, 71^\circ, 109^\circ]$, $[-15^\circ, 195^\circ, 210^\circ, -30^\circ]$, $[199^\circ, -19^\circ, 212^\circ, -32^\circ]$, $[-43^\circ, 223^\circ, 76^\circ, 104^\circ]$, $[7^\circ, 173^\circ, 23^\circ, 157^\circ]$

z -axis are $M = 50$ and $N = 100$, respectively. The densities of ports along the y -axis and z -axis are $\rho_y = \rho_z = 5$. The carrier frequency f utilized in this study is 39 GHz, and we employ the clustered delay line (CDL) channel model as defined by the 3rd Generation Partnership Project (3GPP) [24]. The channel model includes 37 paths, which comprise a LoS path and 36 NLoS paths. The velocity of UEs ranges from 90 km/h to 150 km/h. Each slot contains 14 OFDM symbols, and the duration of a slot is 1 ms. Each group of 50 time slots has a sampling time. The channel corresponding to this sampling moment T_0 serves as the reference channel for that group time. Furthermore, the reference channel is accessible to the UE. To enhance the quantity and diversity of the training dataset, we conducted simulations of communication channels for 10 UEs positioned in various orientations. During the simulation of each UE, we randomly selected distinct sampling time T_0 within the designated time slot. The specific values of the Root Mean Square (RMS) angular spreads of AOD, EOD, AOA, and EOA for these 10 UEs are shown in Table I. A total of 54,300 samples were collected, with 75% of the dataset allocated for the training set and the remaining 25% designated for the test set.

2) Network and Training Parameters

In the simulation of our model, the forecasting period for the FA moving ports is established at $F = 8$. Concurrently, the duration for the employed channel tables is also designated as $T = 8$. As previously indicated, the dimension of the FA moving port table is set as $N \times M = 100 \times 50$. We employ the smallest version of the GPT-2 model with 768 feature dimensions and utilize only the initial $N_L = 6$ layers of the pre-trained GPT-2 architecture. For the LoRA fine-tuning operation, the value of the reduction ratio is set as $r = 4$. Furthermore, the number of heads of the multi-head attention module employed in our model is $K = 8$. And the dimension is set as $d_{\text{model}} = 768$ in the multi-head attention. The Adam algorithm is employed to update the parameters. The specific simulation parameters of our model can be found in Table II. In the training process of our proposed model with the warm-up aided cosine LR schedule, the learning rate of our model $\alpha_{\text{Port-LLM}}$ undergoes a linear increase from $\alpha_{\text{min}} = 4 \times 10^{-6}$ to $\alpha_{\text{max}} = 1 \times 10^{-3}$ in the initial 20 epochs, known as ‘‘warm-

TABLE II: Hyper-parameters for network training

Port-LLM Parameters	Value	
Learning rate	α_{max}	1×10^{-3}
	α_{min}	4×10^{-6}
Exponential decay rate	$\beta_{\text{Port-LLM}}$	(0.9, 0.99)
Batch size	m_1	200
	m_2	200
Number of epochs	\mathcal{K}	500

up’’, followed by a cosine decrease in the final epochs, as described in Eq. (30).

$$\alpha = \alpha_{\text{min}} + \frac{1}{2} (\alpha_{\text{max}} - \alpha_{\text{min}}) \left(1 + \cos \left(\frac{t - T_{\text{max}}}{T - T_{\text{max}}} \pi \right) \right), \quad (30)$$

where T_{max} and T are the number of warm-up and total epochs, respectively. This warm-up-aided cosine annealing algorithm facilitates rapid convergence of our model in the early stages and prevents it from being stuck in local optima due to high learning rates in later stages.

3) Baselines

To assess the efficacy of our proposed model, we conducted a comparative analysis of various model-based and deep learning-based methods for FA moving port calculations, which served as benchmarks.

- **MPMP** [12]: MPMP is a model-based methodology that employs the FA to tackle challenges associated with mobility, utilizing a matrix pencil approach for predicting mobility ports. In the comparative experiment, the mobility port prediction technique based on MPMP has a one-dimensional mobility area for the FA. This mobility region is oriented along the z -axis, measuring 20λ in size and encompassing a total of 100 ports.
- **Vec Prony** [11]: The Vector Prony-based channel prediction algorithm is also a model-based method. In this approach, a second-order Vec Prony algorithm is utilized.
- **RNN** [16]: RNN is a conventional neural network architecture designed for the analysis of sequential data. In our study, we substituted the pre-trained GPT-2 model integrated into our proposed model with an RNN model. The experimental setup involved the utilization of a two-layer RNN network.
- **LSTM** [17]: LSTM is a specialized form of RNNs that effectively mitigate the issues of gradient vanishing and explosion that are commonly faced by conventional RNNs when handling extended sequences. In our experiment, we employed a two-layer LSTM model as a substitute for the loaded GPT-2 model integrated within our framework.
- **GRU** [18]: GRU is a streamlined adaptation of the LSTM architecture. It is engineered to maintain the capacity of LSTM for managing long-term dependencies while simultaneously decreasing computational complexity and the total number of parameters within the model. Similarly, we implemented a two-layer GRU model as an alternative to the loaded GPT-2 model within our framework.

- **Transformer** [26]: The Transformer is a DL model architecture that departs from conventional recurrent neural network frameworks, including RNN, LSTM, and GRU, by utilizing the attention mechanism exclusively for the processing of sequential data. Its primary advantages include the capacity for parallel training, a robust expressive capability, and an effective means of capturing long-range dependencies. In experiment, we employed a Transformer model as a substitute for the loaded GPT-2 model within our framework. Specifically, this Transformer model consists of an 8-head multi-head attention module, with an input dimension of 768 and an embedding dimension of 512.

4) Performance Metrics

To assess the performance of our proposed model, the NMSE_t is employed to quantify the disparity between the actual channel tables \mathbf{S} and the predicted $\hat{\mathbf{S}}$, as described in Eq. (31). The prediction precision of our model on the test set is measured by the accuracy defined in Eq.(32).

$$\text{NMSE}_t = 10 \log_{10} \left\{ \mathbb{E} \left[\frac{\|\hat{\mathbf{S}} - \mathbf{S}\|^2}{\|\mathbf{S}\|^2} \right] \right\} \text{ (dB)}, \quad (31)$$

$$\text{Accuracy} = \left(1 - \frac{|\hat{\mathbf{S}} - \mathbf{S}|}{|\mathbf{S}|} \right) \times 100\%. \quad (32)$$

Furthermore, to enhance the validation of the predicted moving port of FA at the subsequent time point, we computed the NMSE between the channel associated with the predicted port and the reference channel. This metric is referred to as NMSE_v , defined as

$$\text{NMSE}_v = 10 \log_{10} \left\{ \mathbb{E} \left[\frac{\|\mathbf{h} - \mathbf{h}_{\text{ref}}\|^2}{\|\mathbf{h}_{\text{ref}}\|^2} \right] \right\} \text{ (dB)}. \quad (33)$$

Additionally, we conducted a comparative analysis of the spectral efficiency (SE) derived from our model against the SE achieved through the Vec Prony algorithm and the MPMP algorithm, respectively. It is computed as

$$\text{SE} = \sum_{u=1}^{N_{\text{UE}}} \mathbb{E} \{ \log_2 (1 + \text{SINR}_u) \} \text{ (bps/Hz)}, \quad (34)$$

where N_{UE} is the number of UEs, SINR_u denotes signal-to-interference-and-noise ratio of the u -th UE.

B. Performance Evaluation

Fig. 4 shows the curves of NMSE_t and NMSE_v for the training set and test set as the number of training epochs changes during our model training process. The data illustrated in Fig. 4 reveals that the NMSE between the predicted channel tables and the actual channel tables approaches values below -25 dB for both the training and test datasets as the number of training epochs increases. This convergence signifies a high level of accuracy in the channel table predictions made by our proposed model. Furthermore, during the training process, the NMSE between the predicted channels associated with the moving ports of the FA and the reference channels also

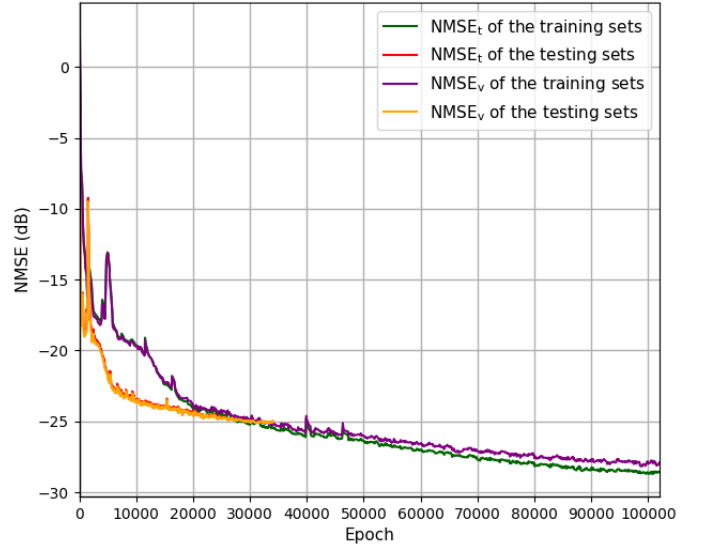


Fig. 4: The NMSE of the proposed Port-LLM model vs. the number of epochs.

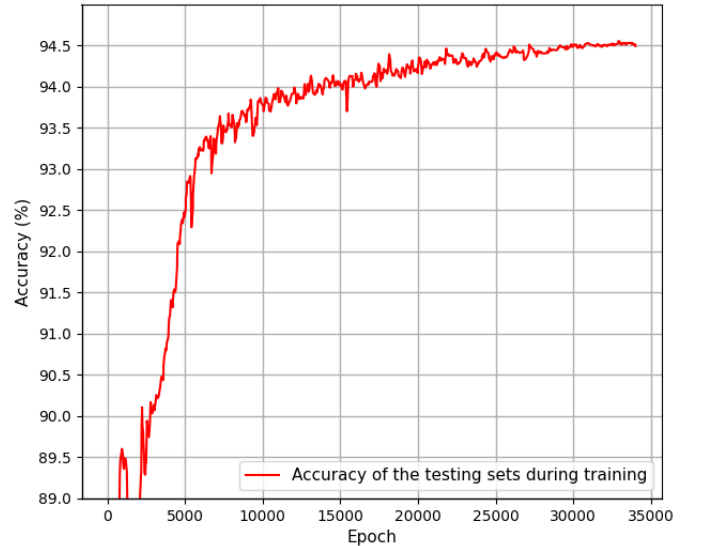


Fig. 5: The prediction accuracy of test datasets during model training.

approaches values below -25 dB for both the training and test sets as the training epochs increase. This finding indicates that the mobile ports of FA, as forecasted by our model, exhibit a high degree of accuracy. By repositioning the FA to the ports predicted by our model, it is feasible to maintain the channel in a nearly unaltered state. Fig. 5 shows the accuracy of the predicted channel tables generated by our model as it varies with the number of training epochs. From the figure, it can be seen that the accuracy of the channel tables predicted by our model is approximately 94.5%.

In practical applications addressing mobility challenges, it is common for BS antennas to be configured as multi-antenna systems. In order to verify the effectiveness of our model in the MISO system, we investigated the performance of our model at 2×8 , 8×8 , and 32×8 antenna configurations at the BS-

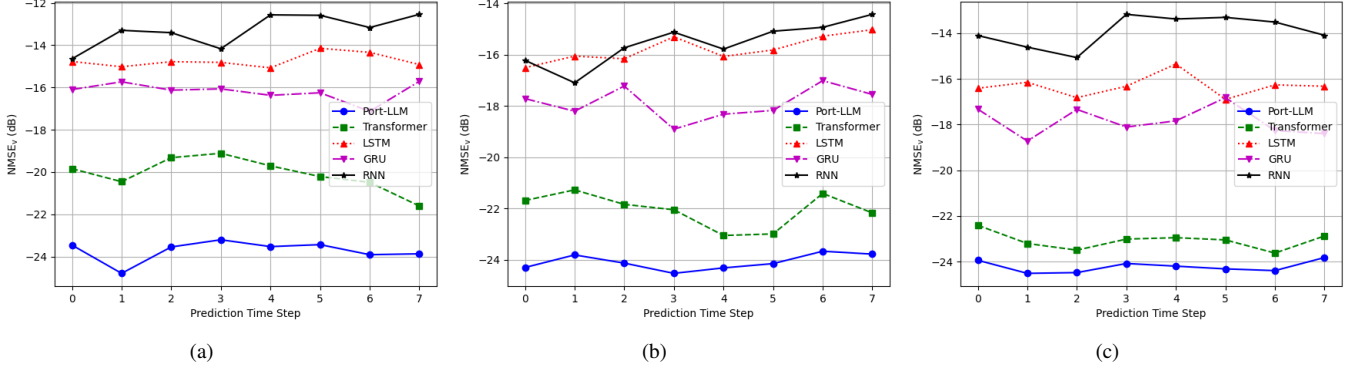


Fig. 6: When the number of antennas on the BS side is 2×8 , the performance of different models under various velocities. (a) The test velocity is 90 km/h; (b) The test velocity is 120 km/h; (c) The test velocity is 150 km/h.

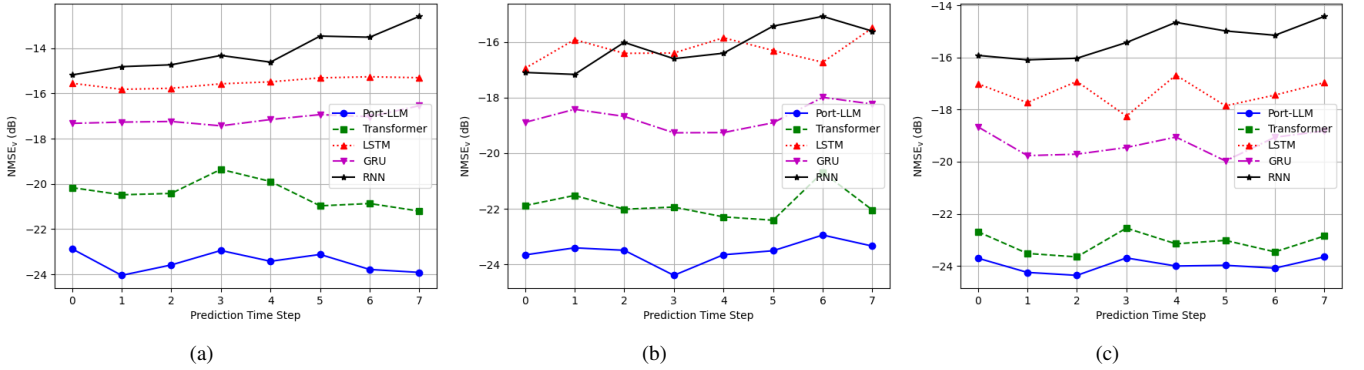


Fig. 7: When the number of antennas on the BS side is 8×8 , the performance of different models under various velocities. (a) The test velocity is 90 km/h; (b) The test velocity is 120 km/h; (c) The test velocity is 150 km/h.

side. Additionally, we compared the prediction performance and robustness of our proposed model against other neural network-based models, taking into account different configurations of BS antennas and varying UE mobility speeds.

Fig. 6, Fig. 7, and Fig. 8 provide a comparative analysis of the efficacy of our model in predicting FA moving ports relative to four other neural network-based models. This evaluation was conducted across three distinct BS antenna configurations and three varying UE mobility speeds. The horizontal axis of the figures denotes 8 consecutive prediction moments, while the vertical axis represents the NMSE between the predicted channels of moving ports and the reference channels. In each scenario, UE data was collected from 10 different orientations, with each UE contributing data over 50 consecutive moments, specifically sampling at the 7-th moment within each time period. The NMSE values predicted by the model were subsequently averaged across all data. The analysis presented in these figures indicates that our model exhibits superior predictive performance, surpassing that of the Transformer-based model. In contrast, the predictive capabilities of the RNN-based, LSTM-based, and GRU-based models are relatively constrained. This deficiency can be attributed to the limited modeling capabilities of RNN-based,

LSTM-based, and GRU-based architectures when addressing complex sequential challenges. Notably, the NMSE between the channel of the mobile port predicted by our model and the reference channel is approximately -24 dB.

Similarly, with a BS antenna configuration of 2×8 and 10 UEs considered, we conducted a comparative analysis of the SE achieved by our proposed model against the SE derived from both the Vec Prony algorithm and the MPMP algorithm. Additionally, we also evaluated the SE under the idealized scenario (“Stationary channel”) and the absence of channel prediction (“No Prediction”). As illustrated in Fig. 9, Fig. 10, and Fig. 11, optimal performance is observed under “Stationary channel” condition. Conversely, performance is significantly diminished in the “No Prediction” condition. Furthermore, the consideration of a two-dimensional (2D) region for FA movement in our model, as opposed to the one-dimensional (1D) framework utilized by the MPMP algorithm, further enhances the performance of our model. As can be observed from these figures, the SE derived from the ports predicted by our model surpasses that obtained from both the Vec Prony algorithm and the MPMP algorithm at medium and high speeds.

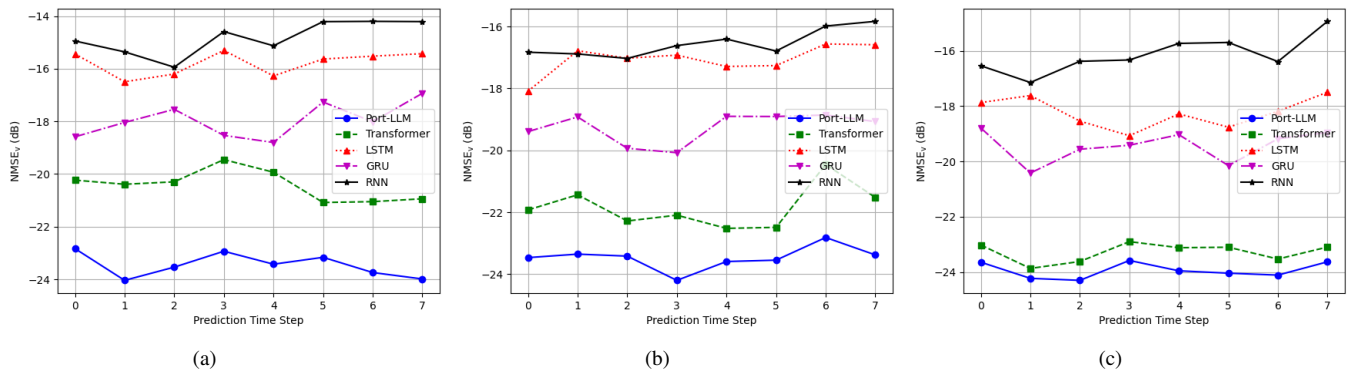


Fig. 8: When the number of antennas on the BS side is 32×8 , the performance of different models under various velocities. (a) The test velocity is 90 km/h; (b) The test velocity is 120 km/h; (c) The test velocity is 150 km/h.

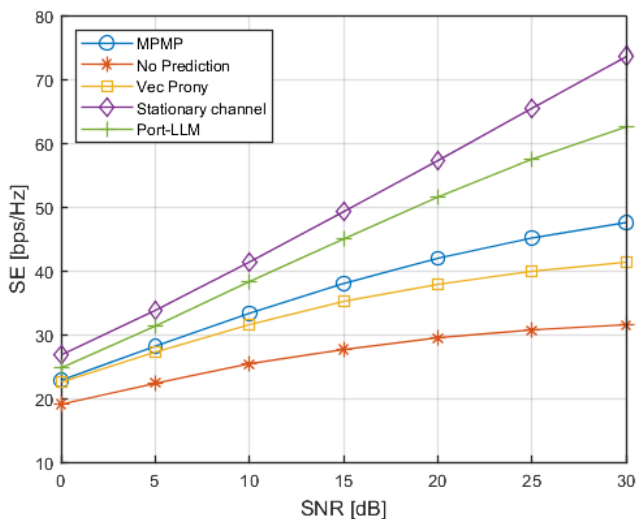


Fig. 9: The SE versus SNR, the BS has 16 antennas, the velocity of UE is 90 km/h.

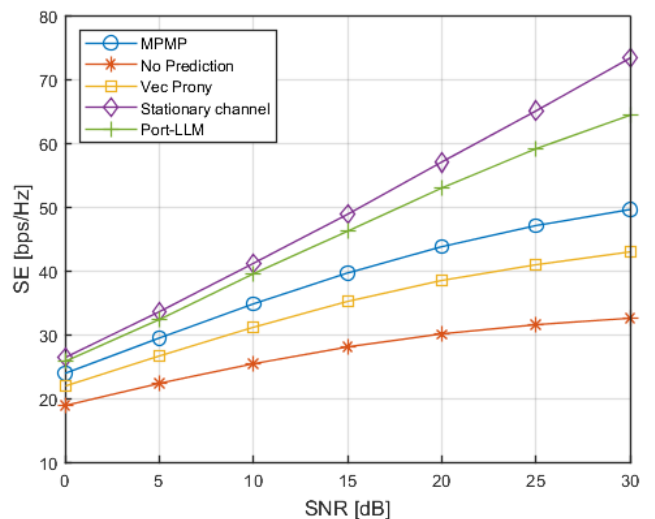


Fig. 10: The SE versus SNR, the BS has 16 antennas, the velocity of UE is 120 km/h.

V. CONCLUSIONS

In this paper, the FA is employed to mitigate the mobility-induced challenges in communication systems. Notably, leveraging the power of the LLMs, we present a moving port prediction model for the FA, designated as Port-LLM. To the best of our current knowledge, this study represents the first application of neural networks to moving port prediction within the domain of FA. By repositioning the FA to the port forecasted by our proposed model, it becomes feasible to maintain an approximately invariant channel state information as the UE moves. The port prediction approach based on our Port-LLM model primarily consists of two sequential steps: the first step involves predicting the channel table, while the second step pertains to port prediction. Furthermore, during the training phase of the Port-LLM model, we incorporated LoRA fine-tuning, which substantially curtailed the number of parameters necessitating retraining. We introduced the warm-up-aided cosine LR technique to improve the prediction accuracy

and convergence speed of our model. Simulation findings indicate that our proposed model exhibits pronounced performance enhancements compared to traditional techniques, particularly in medium and high-speed scenarios. Concurrently, our model demonstrates strong robustness under diverse BS antenna configurations and varying UE movement velocities.

REFERENCES

- [1] K.-K. Wong, A. Shojaeifard, K.-F. Tong, and Y. Zhang, "Fluid Antenna Systems," *IEEE Trans. Wireless Commun.*, vol. 20, no. 3, pp. 1950–1962, 2021.
- [2] Z. Chai, K.-K. Wong, K.-F. Tong, Y. Chen, and Y. Zhang, "Port Selection for Fluid Antenna Systems," *IEEE Commun. Lett.*, vol. 26, no. 5, pp. 1180–1184, 2022.
- [3] K. K. Wong, A. Shojaeifard, K.-F. Tong, and Y. Zhang, "Performance Limits of Fluid Antenna Systems," *IEEE Commun. Lett.*, vol. 24, no. 11, pp. 2469–2472, 2020.
- [4] Y. Huang, L. Xing, C. Song, S. Wang, and F. Elhouni, "Liquid Antennas: Past, Present and Future," *IEEE Open J. Antennas Propag.*, vol. 2, pp. 473–487, 2021.
- [5] L. Zhu and K.-K. Wong, "Historical review of fluid antenna and movable antenna," *arXiv preprint arXiv:2401.02362*, 2024.

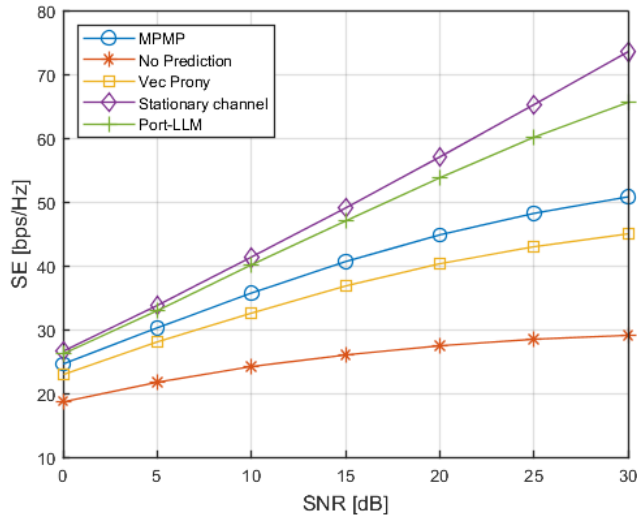


Fig. 11: The SE versus SNR, the BS has 16 antennas, the velocity of UE is 150 km/h.

- [6] L. Zhu, W. Ma, and R. Zhang, "Movable antennas for wireless communication: Opportunities and challenges," *IEEE Commun. Mag.*, vol. 62, no. 10, pp. 114–120, 2023.
- [7] K.-K. Wong, W. K. New, X. Hao, K.-F. Tong, and C.-B. Chae, "Fluid Antenna System—Part I: Preliminaries," *IEEE Commun. Lett.*, vol. 27, no. 8, pp. 1919–1923, 2023.
- [8] K.-K. Wong, K.-F. Tong, and C.-B. Chae, "Fluid Antenna System—Part II: Research Opportunities," *IEEE Commun. Lett.*, vol. 27, no. 8, pp. 1924–1928, 2023.
- [9] L. Zhu, W. Ma, B. Ning, and R. Zhang, "Movable-Antenna Enhanced Multiuser Communication via Antenna Position Optimization," *IEEE Trans. Wireless Commun.*, vol. 23, no. 7, pp. 7214–7229, 2024.
- [10] W. Ma, L. Zhu, and R. Zhang, "MIMO Capacity Characterization for Movable Antenna Systems," *IEEE Trans. Wireless Commun.*, vol. 23, no. 4, pp. 3392–3407, 2024.
- [11] H. Yin, H. Wang, Y. Liu, and D. Gesbert, "Addressing the curse of mobility in massive MIMO with prony-based angular-delay domain channel predictions," *IEEE J. Sel. Areas Commun.*, vol. 38, no. 12, pp. 2903–2917, 2020.
- [12] W. Li, H. Yin, F. Fu, Y. Cao, and M. Debbah, "Transforming Time-Varying to Static Channels: The Power of Fluid Antenna Mobility," *arXiv preprint arXiv:2408.04320*, 2024.
- [13] A. Maatouk, N. Piovesan, F. Ayed, A. D. Domenico, and M. Debbah, "Large Language Models for Telecom: Forthcoming Impact on the Industry," *IEEE Commun. Mag.*, pp. 1–7, 2024.
- [14] Y. Zhang, H. Yin, and L. Han, "A Superdirective Beamforming Approach based on MultiTransUNet-GAN," *IEEE Trans. Commun.*, pp. 1–1, 2024.
- [15] J. Joung, "Machine Learning-Based Antenna Selection in Wireless Communications," *IEEE Commun. Lett.*, vol. 20, no. 11, pp. 2241–2244, 2016.
- [16] Z. C. Lipton, "A Critical Review of Recurrent Neural Networks for Sequence Learning," *arXiv Preprint, CoRR, abs/1506.00019*, 2015.
- [17] S. Hochreiter and J. Schmidhuber, "Long Short-Term Memory," *Neural Computation*, vol. 9, no. 8, pp. 1735–1780, 1997.
- [18] J. Chung, C. Gulcehre, K. Cho, and Y. Bengio, "Empirical evaluation of gated recurrent neural networks on sequence modeling," *arXiv preprint arXiv:1412.3555*, 2014.
- [19] A. Radford, J. Wu, R. Child, D. Luan, D. Amodei, I. Sutskever *et al.*, "Language models are unsupervised multitask learners," *OpenAI blog*, vol. 1, no. 8, p. 9, 2019.
- [20] S. Fan, Z. Liu, X. Gu, and H. Li, "Csi-LLM: A Novel Downlink Channel Prediction Method Aligned with LLM Pre-Training," *arXiv preprint arXiv:2409.00005*, 2024.
- [21] B. Liu, X. Liu, S. Gao, X. Cheng, and L. Yang, "LLM4CP: Adapting Large Language Models for Channel Prediction," *J. Commun. Inf. Networks*, vol. 9, no. 2, pp. 113–125, 2024.
- [22] Y. Sheng, K. Huang, L. Liang, P. Liu, S. Jin, and G. Y. Li, "Beam prediction based on large language models," *arXiv preprint arXiv:2408.08707*, 2024.
- [23] E. J. Hu, Y. Shen, P. Wallis, Z. Allen-Zhu, Y. Li, S. Wang, L. Wang, and W. Chen, "Lora: Low-rank adaptation of large language models," *arXiv preprint arXiv:2106.09685*, 2021.
- [24] 3GPP, *Study on channel model for frequencies from 0.5 to 100 GHz (Release 16)*. Technical Report TR 38.901, available: <http://www.3gpp.org>, 2019.
- [25] A. Vaswani, N. Shazeer, N. Parmar, J. Uszkoreit, L. Jones, A. N. Gomez, L. Kaiser, and I. Polosukhin, "Attention is All you Need," in *Advances in Neural Information Processing Systems 30: Annual Conference on Neural Information Processing Systems (NIPS)*, Long Beach, CA, USA, Dec. 2017, pp. 5998–6008.
- [26] A. Dosovitskiy, L. Beyer, A. Kolesnikov, D. Weissenborn, X. Zhai, T. Unterthiner, M. Dehghani, M. Minderer, G. Heigold, S. Gelly, J. Uszkoreit, and N. Houlsby, "An Image is Worth 16x16 Words: Transformers for Image Recognition at Scale," in the *9th International Conference on Learning Representations (ICLR)*, Vienna, Austria, May, 2021, pp. 1–22.